applied sciences

MDPI

Article

A Mathematical Model of Industrial Waste-Derived Fuel Droplet Combustion in High-Temperature Air

Dmitrii Antonov [1], Dmitrii Glushkov [1,*], Kristina Paushkina [1], Daria Kuznechenkova [1] and Anand Ramanathan [2]

[1] Heat Mass Transfer Laboratory, National Research Tomsk Polytechnic University, Tomsk 634050, Russia
[2] Department of Mechanical Engineering, National Institute of Technology Tiruchirappalli, Tiruchirappalli 620015, India
* Correspondence: dmitriyog@tpu.ru; Tel.: +7-3822-701-777 (ext. 1953)

Abstract: The results of a theoretical and experimental study of the processes of ignition and combustion of a single composite liquid fuel (CLF) droplet based on wet coal processing waste and combustible municipal solid waste under radiant and convective heating are presented. Based on the results of a detailed analysis of video recordings and previously obtained experimental data from the ignition and combustion of a single CLF droplet, a mathematical model was developed. The advantage of the developed mathematical model lies in the specification of sequential physical and chemical processes of the high-temperature decomposition of fuel in a high-temperature gaseous medium. A numerical simulation of combustion characteristics was carried out in the Ansys Fluent commercial software for five different CLF compositions. The ignition-delay times were established for fuel droplets that were in a preheated motionless air environment, a temperature in the range of 723–1273 K, and an air flow heated to 723–973 K moving at a velocity of 3 m/s. Using the asymptotic procedure, satisfactory analytical solutions are obtained for the multistage nonlinear problem of ignition and combustion of a single CLF droplet. The possibility for the practical application of the developed program in Ansys Fluent in predicting the characteristics of the ignition processes of CLF droplets is substantiated.

Keywords: waste; fuel composition; heated air; combustion; numerical simulation

Citation: Antonov, D.; Glushkov, D.; Paushkina, K.; Kuznechenkova, D.; Ramanathan, A. A Mathematical Model of Industrial Waste-Derived Fuel Droplet Combustion in High-Temperature Air. *Appl. Sci.* **2022**, *12*, 12273. https://doi.org/10.3390/app122312273

Academic Editor: Matt Oehlschlaeger

Received: 27 October 2022
Accepted: 28 November 2022
Published: 30 November 2022

1. Introduction

The current hazards of fossil fuel depletion in the medium term and of irreversible climate change due to global warming have prompted the design and implementation of sustainable development policy in the main areas of the economy. Quickly growing population, rapid industrialization and global economic changes have increased the demand for electric and thermal energy [1] even as there is a projected deficit of energy resources and fossil fuels. According to the industry estimates [2], even though there was a decrease in the energy demands during the COVID-19 pandemic, humanity is expected to consume 10% more primary energy in 2030 (and 35% more in 2050) compared to the annual consumption in 2019.

Coal energy production is a globally widespread technology that generated about seven billion tons of industrial waste in 2020 alone [3], and this figure is projected to rise to 25 billion tons by 2026 [4]. In addition to industrial waste, municipal waste (including combustible waste) pollutes the environment. According to estimates [5], if humanity annually produced 2.1 billion tons of municipal solid waste (MSW) in 2019, then by 2050 people will generate about 3.4 billion tons. Stored at open-air disposal sites, industrial and municipal solid wastes pollute the environment (air, soil and water) as a result of their slow natural decay [5,6]. Overall, this leads to deteriorating conditions for both people and wildlife living in the vicinity [7–10].

One of the most economically sparing ways to utilize accumulated and unclaimed waste is the method of burning composite liquid fuels (CLF). The results of a cycle of

experimental research [11–13] into the combustion of CLF, consisting of wet coal enrichment waste (high-moisture low-rank coal) and fine MSW, have proved the efficiency of using the waste-to-energy technology to generate heat and power with a relatively low level of anthropogenic emissions.

The use of such CLFs in practice is limited by the need to develop a number of compositions with predictable energy characteristics. The scientific justification of a high-potential fuel component composition is time-consuming, costly and challenging. The numerical simulation of physical and chemical processes is an alternative approach to the efficient prediction of fuel combustion characteristics under different conditions.

In recent years, many mathematical models have been developed to study the influence of environmental conditions and fuel properties on the thermal decomposition characteristics of different grades of coal [14,15] and a group of typical MSW components taken separately [16–19]. Studies on the modeling of MSW thermal decomposition for subsequent practical application generally state the problem with significant assumptions and simplifications, which increases the scale of the problem to be solved and lowers the requirements of the numerical simulation algorithm for the PC's computational resources. Yet this approach does not make it possible to explore the physics and chemistry of solid fuel conversion. Studies like that may use empirical models of the conversion of solid fuel in a densified layer divided into several zones (e.g., drying, pyrolysis, combustion, gasification), to estimate the qualitative and quantitative characteristics of gaseous pyrolysis and gasification products [18].

In a number of works [17,19], the Eulerian–Lagrangian model is used. It describes gas (liquid) flows with a low content of the dispersed phase [20,21]. Solid fuel particles are considered as a discrete phase (Lagrangian), and gas (liquid) flows are considered as a continuous medium (Eulerian). However, the Eulerian–Lagrangian approach is not suitable for modeling the processes in suspensions, fluidized bed layers and any other mixtures in which the volume ratio of the solid phase cannot be neglected. Fuel conversion in the fluidized bed is described using the Eulerian–Eulerian model (continuum model) [16,22], which describes different phases as continuous media. Such a simplified approach makes it possible to reliably predict the temperature fields and velocity profiles, though it is not relevant for an in-depth study of heat and mass transfer, as well as hydrodynamics processes developing in a single fuel particle and in its vicinity.

Analysis of the synergistic effect of the components of the CLF mixture (coal, water and MSW) on the temporal and environmental characteristics of the fuel combustion is a promising direction with significant potential for the development of previously obtained experimental research findings [23]. Therefore, the aim of this work is to develop, on the basis of the results of previous experimental studies [23,24], a mathematical model for the combustion of a unit multicomponent CLF droplet in an air medium heated to high temperatures, which provides a satisfactory reproduction of the experimental data. The model is supposed to intensify research in the field of eco-energy and to develop a strategy for the sustainability of the electric power industry with limited consumption of exhaustible natural resources and minimal negative impact on the environment.

2. Materials and Methods

2.1. Background of the Model Condition

The ability of CLS to reliably ignite and burn out completely in a preheated gaseous medium has been established by us experimentally [23]. The identified mechanism and recorded characteristics of the process set the stage for the development of the mathematical model and numerical simulation of single fuel droplet combustion in Ansys Fluent. The main component of the CLF was filter cake (FC) of coking coal C from the Severnaya coal plant (Kuzbass, Russian Federation) [23]. FC is a waste from the coal industry, obtained in the process of coal enrichment. FC has an energy potential due to the content of at least 50% fine (about 100 μm) coal in the composition (the rest is water) [25–27]. However, so far, FC is not widely used in any industries, so the main method of its disposal is uncontrolled

storage on open sites near the washing plant. This method of coal waste disposal is characterized by many negative consequences, primarily environmental. Moisture evaporation increases the fire hazard of coal dust, allows it to be dispersed by the wind over large areas, polluting the air, open water bodies and soils. Moreover, coal dust contains acidifying agents, high-density metals and other hazardous elements. These become a source of integrated pollution for the environment, when exposed to a severe impact of natural factors (such as air, moisture or solar energy).

Besides FC, combustible MSW can also be a CLF component [23,28]. MSW typically consists [5,29,30] of 26–35% organic remains (including former foodstuff); 25–30% (of the total waste volume) mixed paper wastage; 7–10% postconsumer plastics; 5–12% scrap metal and cullet; 2–4% textile wastes, 2–4% wood residue, and 2–4% all-rubber scraps. Based on statistical data, MSW consists of about 82% potentially energy-producing materials (paper, wood, textile, polymer waste). Adding the combustible components of MSW to composite fuel is a promising solution to the problem of commercial disposal of accumulated and newly produced waste. However, the relatively low energy content of combustible MSW (10 MJ/kg [31–33] versus 20–30 MJ/kg [34] of solid fossil fuels) and a fairly high concentration of hazardous compounds (including carcinogens) limit the amount that can be added to a CLF composition to 10–20% [23].

The main properties, characteristics and ultimate analysis of CLF are presented in Tables 1 and 2 [28]. To obtain the characteristics and properties of the CLF components, the samples were preliminarily dried at a temperature of about 378 K to evaporate unbound moisture.

Table 1. Characteristics and properties of composite liquid fuel components [28].

Component	W^a (%)	A^d (%)	V^{daf} (%)	$Q^a_{s,V}$ (MJ/kg)	Specific Heat Capacity (kJ/(kg·K))	Thermal Conductivity (W/(m·K))
Filter cake C (dry)	-	26.50	23.10	24.83	1.30	0.366
Wood	20.00	2.00	83.10	16.45	1.55	0.200
Rubber	2.00	1.80	67.40	33.50	1.38	0.150
Plastic	2.00	0.20	99.50	22.00	2.30	0.260
Cardboard	5.00	3.00	96.57	17.50	2.30	0.130

Table 2. Ultimate analysis of composite liquid fuel components [28].

Component	C^{daf} (%)	H^{daf} (%)	N^{daf} (%)	S^{daf} (%)	O^{daf} (%)
Filter cake C (dry)	87.20	5.10	2.10	1.10	4.50
Wood	50.30	6.00	0.20	0.10	43.40
Rubber	97.90	1.20	0.30	0.60	-
Plastic	66.70	7.90	-	-	25.40
Cardboard	46.30	6.30	0.30	0.20	46.90

In the experimental research [23], MSW characteristics from reference materials were used to analyze the effect of CLF component properties on the patterns of physical and chemical processes with different mechanisms of heat supply [31,35,36]. MSW composition and characteristics may vary considerably in different regions (by methods of waste collection and treatment, as well as storage conditions) [5]. To predict the characteristics of CLF droplet ignition and combustion reliably, it is necessary to use the real properties of solid particles and liquids included in the fuel mixture (primarily thermophysical and kinetic characteristics of phase transitions and chemical transformations). An undoubted advantage of modeling is that the component composition fuel suspension, droplet sizes, heat transfer mechanisms and characteristics of heat supply from the external source can be varied in wide ranges. Thus, it is possible to efficiently assess the potential of using promising fuel compositions in practice.

In the research, the numerical simulation was carried out for single droplets (with the initial diameter d_p = 1 mm) of five different CLF compositions based on wet FC with MSW: No. 1—FC 100%; No. 2—FC 90% + wood 10%; No. 3—FC 90% + rubber 10%; No. 4—FC 90% + plastic 10%; No. 5—FC 90% + cardboard 10%.

Adding 10% of MSW corresponds to the experimental findings [11,23,28,37] that established that 5–20% of typical combustible MSW added to the CLF composition does not affect the its mechanisms or energy characteristics. At the same time, based on the estimates [38], adding 10–20% typical MSW to the CLF composition will reduce the area of land excluded from agricultural use due to landfill site arrangements by 20–30%. It will also save depleting fossil fuels burned for heat and power generation.

2.2. Experimental Data

The experimental research [23] into the ignition and combustion of single CLF droplets was conducted on two different test installations. The first condition [23] (Figure 1a) created the radiation-supported heating conditions of a suspended droplet in a tubular muffle furnace ($V_g \approx 0$) with a temperature varying in the range of 723–1273 K. Using the second condition (Figure 1b), the same fuel droplet was heated convectively with hot air at a velocity of $V_g \approx 3$ m/s, the air temperature varied within a range of 723–973 K [23]. The second experimental condition (Figure 1b), in laboratory conditions, simulated the interaction processes of fuel droplets with a stream of hot air, which are the basis of industrial technologies for the flaring of liquid and solid fuels [39].

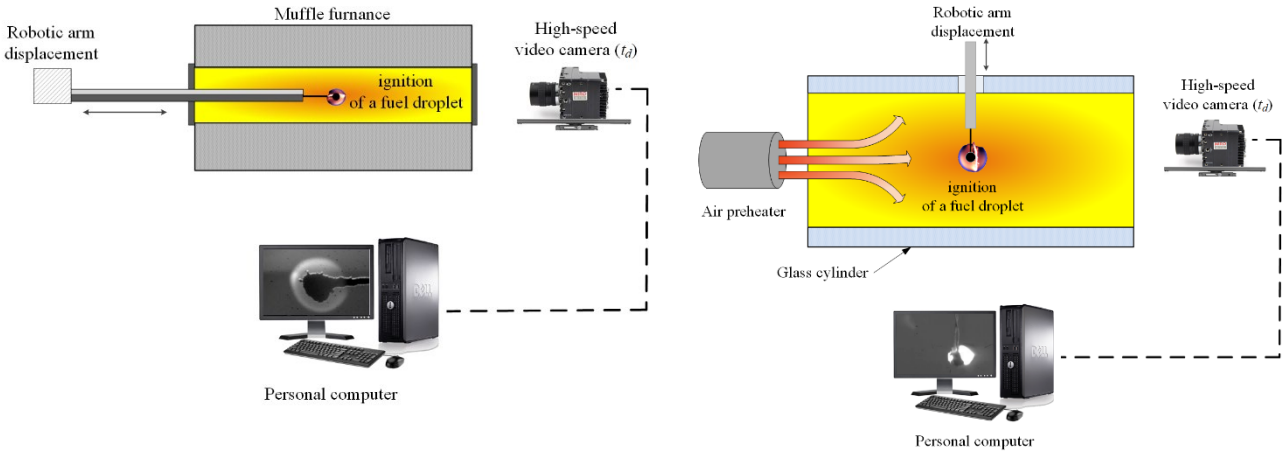

Figure 1. Schematic of experimental conditions: (**a**) first condition; (**b**) second condition.

Carrying out experiments on the demonstrated conditions [23] made it possible to comprehensively analyze the effect of various heating conditions on the ignition characteristics of CLF droplets (Figure 2). The characteristics of ignition under near-critical conditions substantially depend on the patterns of phase transitions and the mechanism of heat and mass transfer for various methods of heat supply to the CLF droplet [40]. Fuel droplets exposed to radiant (Figure 2a) and convective (Figure 2b) heating feature identical patterns of physical and chemical processes. Conditionally the following sequence of basic reaction phases of a CLF droplet and warmed-over air (moving and motionless) can be distinguished: passive warming, near-surface water vaporization, thermolysis of coal and municipal waste (solid combustible components), blending of ignitable gases with the oxidizing medium, gas blend firing and burnout, heating of the solid remainder and finally its heterogeneous ignition and combustion. The main difference between the processes presented in the video frames (in Figure 2a,b) is in the significantly longer passive warming of the fuel droplet and formation of a combustible gas mixture mainly due to the diffusion of volatiles in the oxidizer medium in the vicinity under radiant heating conditions (Figure 2a).

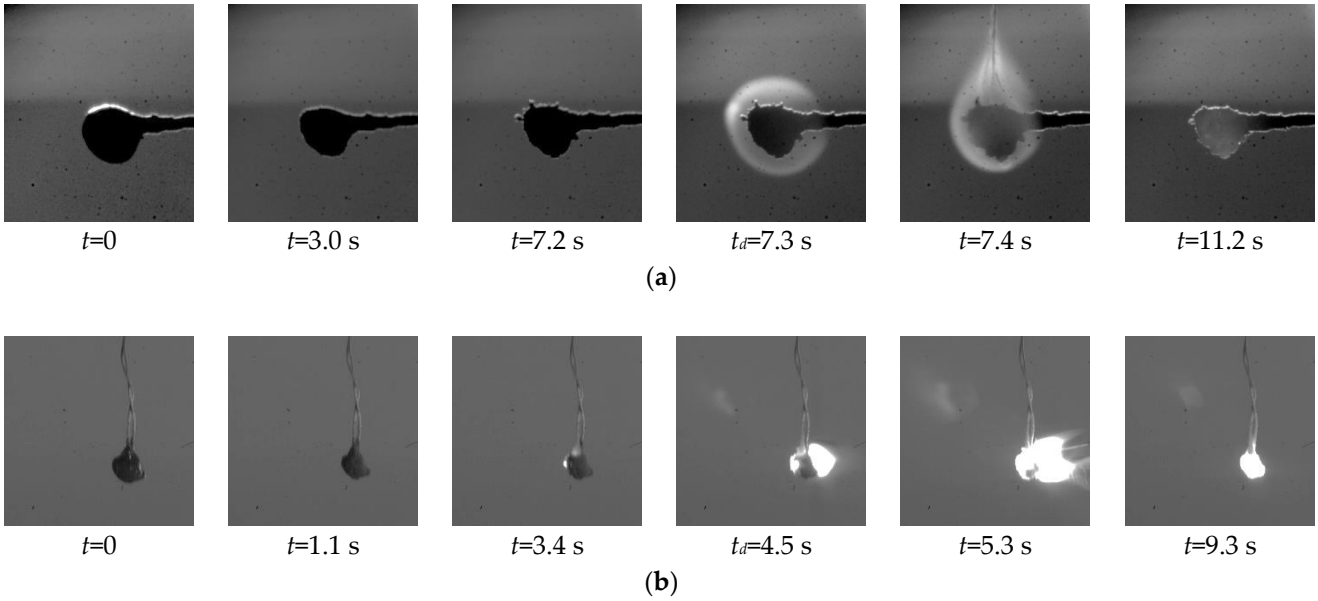

Figure 2. Video frames of ignition and combustion of CLF droplets No. 5 (FC 90% + cardboard 10%) at T_g = 873 K [23] under the following conditions: (**a**) radiant heating ($V_g \approx 0$); (**b**) convective heating ($V_g \approx 3$ m/s).

In the experimental research (Figure 2) [23], the ignition-delay times (t_d) were determined using the commercial Tema Automotive software (Image Systems AB, Sweden) and the built-in Threshold algorithm by the variation of the luminance around the droplet over time [11]. The systematic error of the measuring system in determining the ignition-delay time is less than 3%. Random errors of a series of five repeated measurements under the same experimental conditions are less than 10%. The main experimental values [23] of the average t_d of droplets (with the initial diameter d_p = 1 mm) of CLF with the addition of various MSW at different air temperatures under conditions of dominant radiant and convective heating are presented in Tables 3 and 4. The calculation results for the developed model will be validated by comparison with these experimental data.

Table 3. Average ignition-delay times of CLF exposed to radiant heating ($V_g \approx 0$) at different air temperatures [23].

No. of Composition	Temperature of Motionless Air ($V_g \approx 0$)						
	723 K	**773 K**	**873 K**	**973 K**	**1073 K**	**1173 K**	**1273 K**
No. 1	19.57	16.32	11.39	8.14	5.90	4.13	2.98
No. 2	18.15	15.04	10.47	7.50	5.26	3.77	2.69
No. 3	17.00	14.08	9.67	6.74	4.65	3.29	2.31
No. 4	16.55	13.60	9.19	6.26	4.25	2.98	2.02
No. 5	14.15	11.35	7.30	4.62	2.85	1.73	0.96

Table 4. Average ignition-delay times of CLF exposed to convective heating ($V_g \approx 3$ m/s) at different air temperatures [23].

No. of Composition	Air-Flow Temperature ($V_g \approx 3$ m/s)					
	723 K	**773 K**	**823 K**	**873 K**	**923 K**	**973 K**
No. 1	7.48	6.00	4.86	3.93	3.14	2.56
No. 2	7.03	5.62	4.53	3.65	2.89	2.36
No. 3	6.65	5.38	4.38	3.53	2.81	2.31
No. 4	6.54	5.28	4.26	3.43	2.71	2.19
No. 5	6.37	5.15	4.14	3.34	2.65	2.14

2.3. Mathematical Model

The structure of CLF is a rather complex system. When CLFs are heated, a set of interdependent processes, phase transformations and chemical reactions occurs [41]: passive warming, near-surface water vaporization, thermolysis of coal and municipal waste (solid combustible components), blending of ignitable gases with the oxidizing medium, gas blend firing and burnout, heating of the solid remainder followed by its heterogeneous ignition and combustion. These processes were described in the development of the mathematical model in Ansys Fluent. The discrete particle model (DPM) for composite fuels has been developed (Eulerian–Lagrangian model).

The gas is defined as a stationary medium. The gas phase is described by a stationary Reynolds-averaged Navier–Stokes (RANS) model (1)–(3) [42].

$$\nabla \cdot \left(\rho \vec{u}\right) = 0 \tag{1}$$

$$\nabla \cdot \left(\rho \vec{u} \vec{u}\right) = -\nabla p + \nabla \cdot (\overline{\tau}) + \rho \vec{g} + \vec{F} \tag{2}$$

$$\nabla \cdot \left[\vec{u}(\rho H + p)\right] = -\nabla \cdot \left(\sum_i h_i J_i\right) \tag{3}$$

where ∇—nabla operator; $\vec{F}$—vector of volumetric fluid–particle interaction force, N; H—enthalpy, W; $\overline{\tau}$—gas viscous stress, Pa; J—mass flux, kg/(m^2·s); h—sensible heat, W; and subscripts i—species.

One of the most important parameters characterizing turbulent motion is turbulent kinetic energy k. The transfer equation for turbulent kinetic energy is derived from the Navier–Stokes and Reynolds equations and is defined as (4):

$$\operatorname{div}\left(\rho k \vec{u}\right) = \operatorname{div}\left[\left(\mu + \frac{\mu_t}{\sigma_k}\right) \operatorname{grad} k\right] + G_k - \rho\varepsilon \tag{4}$$

For finding viscous dissipation ε, the transfer equation (k–ε model) is used (5):

$$\operatorname{div}\left(\rho \varepsilon \vec{u}\right) = \operatorname{div}\left[\left(\mu + \frac{\mu_t}{\sigma_\varepsilon}\right) \operatorname{grad} \varepsilon\right] + C_{\varepsilon 1} \frac{\varepsilon}{k} G_k - C_{\varepsilon 2} \rho \frac{\varepsilon^2}{k} \tag{5}$$

where G_k—the generation of turbulence kinetic energy related to the mean velocity gradient and the turbulent model constants $C_{\varepsilon 1} = 1.44$; $C_{\varepsilon 2} = 1.92$; $\sigma_k = 1$; $\sigma_\varepsilon = 1.3$.

The gas species equation is defined as (6):

$$\nabla \cdot \left(\rho \vec{u} Y\right) = -\nabla \cdot \vec{J} + R_p \tag{6}$$

where ∇—nabla operator; R_p—rate of production, units vary.

The combusting particle is used as a physical model in the discrete particle model (DPM) to define a single CLF droplet in a gaseous flow. The combusting particle is described by a system of the following laws: heating/cooling, release of volatiles, heterogeneous surface combustion [42]. Meanwhile, at each moment of time there is no temperature gradient inside the combustible particle. It is considered a body with an almost uniform temperature distribution.

Since the model is developed for slurry fuel, it is necessary to use a wet combustion model, so the combusting particle has been extended to include the fraction of the liquid component capable of boiling and vaporizing. The vaporization rate is defined as:

$$N_i = k_c(C_{i,s} - C_{i,\infty}) \tag{7}$$

where N_i—molar flux of vapor, kg·mol/(m^2·s); k_c—mass transfer coefficient, m/s; $C_{i,s}$—vapor concentration at the droplet surface, kg·mol/m^3; and $C_{i,\infty}$—vapor concentration in the bulk gas, kg·mol/m^3.

Dalton's law determines the vapor concentration near the surface of a fuel droplet:

$$C_{i,s} = \frac{p_{\text{sat}}(T_p)}{RT_p} \tag{8}$$

where R—the universal gas constant; p_{sat}—pressure of saturated vapor; and T_p—droplet temperature.

The concentration of vapor in the bulk gas is known from the solution to the transport equation for species i for non-premixed or partially premixed combustion calculations:

$$C_{i,\infty} = X_i \frac{p}{RT_\infty} \tag{9}$$

where X_i—the local bulk mole fraction of species i; p—the local absolute pressure; and T_∞—the local bulk temperature in the gas.

The Rantz and Marshall correlation was used to estimate the mass transfer coefficient k_c from the Sherwood number [42]:

$$\text{Sh} = \frac{k_c d_p}{D_{i,m}} = 2.0 + 0.6\text{Re}_d^{\frac{1}{2}}\text{Sc}^{\frac{1}{3}} \tag{10}$$

where Sc—the Schmidt number, $\text{Sc} = \frac{\mu}{\rho D_{i,m}}$.

When moisture evaporates from a droplet, its mass decreases according to the equation:

$$m_p(t + \Delta t) = m_p(t) - N_i A_p M_{w,i} \Delta t \tag{11}$$

where $M_{w,i}$—molecular weight of species i, kg/(mol·K).

The rate of convective boiling of the liquid contained in the droplet after reaching the boiling point (T_{bp}):

$$\frac{d(d_p)}{dt} = \frac{4k_\infty}{p_p c_{p,\infty} d_p}\left(1 + 0.23\sqrt{\text{Re}_d}\right)\ln\left[1 + \frac{c_{p,\infty}(T_\infty - T_p)}{h_{\text{fg}}}\right] \tag{12}$$

The motion equation is described using Newton's second law of motion:

$$\frac{du_p}{dt} = F_D(u - u_p) + \frac{g(\rho_p - \rho)}{\rho_p} + F_a \tag{13}$$

where F_a—additional acceleration, N/kg; $F_D\,(u - u_p)$—drag force, N/kg; and F_D—coefficient in drag law, 1/s.

Coefficient in drag law F_D for a spherical droplet is defined as:

$$F_D = \frac{18\mu}{\rho_p d_p^2}\frac{C_D\text{Re}}{24} \tag{14}$$

where C_D—drag coefficient for spherical droplet.

Relative Reynolds number Re is defined as:

$$\text{Re} = \frac{\rho d_p |u_p - u|}{\mu} \tag{15}$$

The heating of the combusting particle is described by the energy equation:

$$m_p c_p \frac{dT_p}{dt} = hA_p(T_\infty - T_p) + \frac{dm_p}{dt} h_{fg} + A_p \varepsilon_p \sigma \left(\theta_R^4 - T_p^4\right) \quad (16)$$

$$m_p c_p \frac{dT_p}{dt} = hA_p(T_\infty - T_p) - f_h \frac{dm_p}{dt} H_{\text{reac}} + A_p \varepsilon_p \sigma \left(\theta_R^4 - T_p^4\right) \quad (17)$$

Energy equations of particles (16) and (17) are solved analytically, by assuming that the temperature and mass of the particle do not change significantly between time steps [42]:

$$T_p(t + \Delta t) = \alpha_p + \left[T_p(t) - \alpha_p\right] e^{-\beta_p \Delta t} \quad (18)$$

Coefficients of α_p and β_p in equation (18) are defined as:

$$\alpha_p = \frac{hA_p T_\infty + \frac{dm_p}{dt} h_{fg} + A_p \varepsilon_p \sigma \theta_R^4}{hA_p + A_p \varepsilon_p \sigma T_p^3} \quad (19)$$

$$\beta_p = \frac{A_p \left(h + \varepsilon_p \sigma T_p^3\right)}{m_p c_p} \quad (20)$$

where h_{fg}—latent heat, J/kg; H_{reac}—heat released by the surface reaction, J/kg; f_h—particle fraction which absorbs heat of reaction; ε_p—particle emissivity; σ—Stefan–Boltzmann constant, W/(m^2·K^4); and θ_R—radiation temperature, K.

The Rantz and Marshall correlation was also used to estimate the heat transfer coefficient in accordance with the main provisions [43,44], since the CLF droplet is considered as a system with an almost uniform temperature distribution. Convective heat transfer coefficient h is defined from the Nusselt number (21) which is a function of particle Reynolds number (15) and gas Prandtl number:

$$\text{Nu} = \frac{hd_p}{k_\infty} = 2.0 + 0.6 \cdot \text{Re}^{1/2} \text{Pr}^{1/3} \quad (21)$$

$$\text{Pr} = \frac{c_p \mu}{k_\infty} \quad (22)$$

The devolatilization process (23) releases volatiles ($C_\alpha H_\beta O_\gamma N_\delta$) and char ($C_s$) [42]:

$$\text{Solid fuel} \rightarrow C_\alpha H_\beta O_\gamma N_\delta + C_s \quad (23)$$

The rate of devolatilization is determined as a constant value according to the equation [45,46]:

$$-\frac{1}{f_{v,0}(1 - f_{w,0}) m_{p,0}} \cdot \frac{dm_p}{dt} = A_0 \quad (24)$$

where $f_{v,0}$—initial mass fraction of volatiles; $f_{w,0}$—initial mass fraction of evaporating material; $m_{p,0}$—initial particle mass, kg; and A_0—rate constant, s^{-1}.

Note that the volatilization process occurs when the particles of coal reach the evaporation temperature (in our case vaporization temperature is equal to 400 K [47]). Particle swelling effects during devolatilization are ignored, which is consistent with experimental observations [28,41,48]. The change of particle temperature is determined from the energy equations of particles (16) and (17) governed by conductive, convective and radiative heat transfer [42].

The multiple surface reactions model is used for the description of the reacting particle. Any number of chemical reactions can be described using the multiple surface reactions model [42]. The scheme for a reacting particle in the multiple surface reactions model is shown in Figure 3.

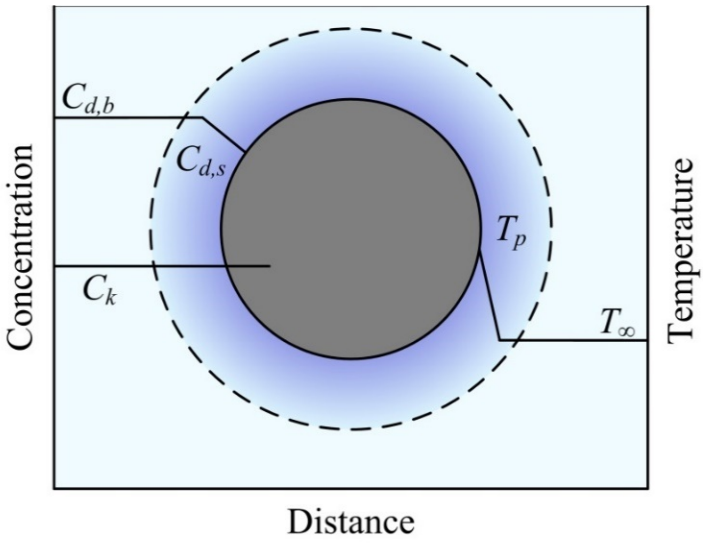

Figure 3. A reacting particle in the multiple surface reactions model [42]: T_p—droplet temperature; $T\infty$—ambient gas temperature; $C_{d,b}$ and $C_{d,s}$—concentration of the diffusion-limited species; C_k—concentrations of all other species.

The rate of chemical reactions:

$$\overline{R}_{j,r} = A_p \eta_r Y_j R_{j,r} \tag{25}$$

$$R_{j,r} = R_{\text{kin},r}\left(p_n - \frac{R_{j,r}}{D_{0,r}}\right)^{N_r} \tag{26}$$

where $\overline{R}_{j,r}$—rate of particle surface species depletion, kg/s; A_p—particle surface area, m^2; η_r—effectiveness factor; $R_{j,r}$—rate of particle surface species reaction per unit area, kg/(m^2·s); p_n—bulk partial pressure of the gas phase species, Pa; $R_{\text{kin,r}}$—kinetic rate of reaction, units vary; $D_{0,r}$—diffusion rate coefficient for reaction; and N_r—apparent order of reaction.

The diffusion rate coefficient $D_{0,r}$ is defined as:

$$D_{0,r} = C_{1,r}\frac{\left[\left(T_p + T_\infty\right)/2\right]^{0.75}}{d_p} \tag{27}$$

The kinetic rate of multiple reactions is defined as:

$$R_{\text{kin},r} = \frac{A_r T_p^{\beta_r} e^{-\left(E_r/RT_p\right)}}{\left(p_{r,d}\right)^{N_r}} \prod_{n=1}^{n_{\max}} p_n^{N_{r,n}} \tag{28}$$

where A_r—pre-exponential factor; β_r—temperature exponent; E_r—activation energy for reaction, J/(mol·K); $p_{r,d}$—bulk partial pressure of the diffusion-limited species, Pa; and subscripts: n—number of gas specie.

The main kinetic parameters of chemical reactions used in the modeling are presented in Table 5.

Table 5. Kinetic parameters of chemical reactions of CLF ignition.

Reaction	A_r	E_r (kJ/(mol·K))	Ref.
Water Evaporation			
$H_2O(l) = H_2O(g)$	$5.13 \cdot 10^6$	87.9	[49,50]
Pyrolysis Biomass pyrolysis			
lignin = $0.209CO_2 + 0.396CO + 0.109H_2 + 0.249H_2O + 0.037$vol	$2.202 \cdot 10^{12}$	181	[50]
hemicellulose = $0.209CO_2 + 0.396CO + 0.109H_2 + 0.249H_2O + 0.037$vol	$2.527 \cdot 10^{11}$	147	[50]
cellulose = $0.209CO_2 + 0.396CO + 0.109H_2 + 0.249H_2O + 0.037$vol	$1.379 \cdot 10^{14}$	193	[50]
Rubber pyrolysis			
rubber = $0.8H_2 + 0.0009C_2H_4 + 0.194CH_4 + 0.0025C_3H_6 + 0.0018C_4H_6 + 0.0008C_2H_2$	$5.5 \cdot 10^{18}$	181	[51,52]
Plastic pyrolysis			
polyethylene = $0.825H_2 + 0.07C_2H_4 + 0.05CH_4 + 0.03C_3H_6 + 0.02C_2H_6 + 0.005C_3H_8$	$15 \cdot 10^3$	40	[53]
Gasification			
$C + H_2O = CO + H_2$	$2.07 \cdot 10^7$	220	[50,54–56]
$C + CO_2 = 2CO$	$1.32 \cdot 10^7$	259	[50,55–59]
$C + 2H_2 = CH_4$	$5 \cdot 10^6$	30	[50,55,56,58]
$C + 2H_2O = CO_2 + 2H_2$	$2.1 \cdot 10^6$	158	[50,57,60]
$CO_2 + H_2 = CO + H_2O$	$5 \cdot 10^6$	30	[49,58,61]
Combustion			
$C + O_2 = CO_2$	$2 \cdot 10^{12}$	60.6	[55,57,62]
$C + 1/2O_2 = CO$	$2 \cdot 10^{12}$	60.6	[55,57–59]
$H_2 + 1/2O_2 = H_2O$	$2.1 \cdot 10^{14}$	129.8	[54,55,58]
$2CO + O_2 = 2CO_2$	$1.4 \cdot 10^{13}$	96.8	[54,55,58]
$CO + H_2O = H_2 + CO_2$	$5 \cdot 10^6$	30	[55,56,58]
$CO + 3H_2 = CH_4 + H_2O$	$5 \cdot 10^6$	30	[49]
$C + H_2O = 1/2CO_2 + 1/2CH_4$	$5.6 \cdot 10^{12}$	36.2	[49,63]
$CH_4 + 2O_2 = CO_2 + 2H_2O$	$5.6 \cdot 10^{12}$	103.8	[58,64]
$C_2H_4 + O_2 = 2CO + 2H_2$	$1 \cdot 10^{12}$	173	[21]
$2C_3H_6 + 9O_2 = 6CO_2 + 6H_2O$	$1.51 \cdot 10^{15}$	85.6	[65]
$2C_2H_6 + 7O_2 = 4CO_2 + 6H_2O$	$1.1 \cdot 10^{12}$	125.52	[66]
$2C_3H_8 + 10O_2 = 6CO_2 + 8H_2O$	$8.6 \cdot 10^{11}$	125.52	[66]
$C_4H_6 + 3O_2 = 4CO + 2H_2O + H_2$	$8.8 \cdot 10^{11}$	126.37	[67,68]
$C_4H_8 + 1/2O_2 = C_2H_4 + H_2O$	$6 \cdot 10^{12}$	502	[67]
$C_4H_8 + 6O_2 = 4CO_2 + 4H_2O$	$3 \cdot 10^7$	10.4	[67]
$C_4H_6 + 11/2O_2 = 4CO_2 + 3H_2O$	$3 \cdot 10^7$	10.4	[67]
$C_2H_2 + O_2 = 2CO + H_2$	$6 \cdot 10^{13}$	50	[69]

The thermophysical and transport properties of multi-component CLF droplets, which are a heterogeneous mixture of coal, water and MSW, were set as effective values, which were determined analytically using the method [70] based on the data presented in Tables 3 and 4. The obtained values are presented in Table 6.

For the developed model of CLT droplet ignition under different heating conditions, a structured rectangular grid 30 × 30 mm in size was generated using ANSYS Fluent [42]. To assess the influence of the grid element sizes on the simulation results, a series of calculations was carried out with a gradual increase in the number of elements. The calculations were carried out for grids consisting of 5625, 14,400 and 360,000 elements (Table 7). The grid convergence index (GCI) was calculated according to the recommended procedure for the estimation of discretization errors [71,72]. The number of elements and the charac-

teristic size of the computational grid were considered optimal when the corresponding convergence criteria were met (GCI $\leq$ 0.05%). Grid 2 satisfies this condition (Table 7).

Table 6. The main characteristics of different CLF compositions.

Characteristics	No. of Composition				
	No. 1	**No. 2**	**No. 3**	**No. 4**	**No. 5**
Q (MJ/kg)	10.78	11.29	13.05	11.88	11.43
Specific heat capacity (kJ/(kg·K))	2.4600	2.4175	2.3549	2.4136	2.4136
Thermal conductivity (W/(m·K))	0.4796	0.4582	0.4550	0.4620	0.4547
Viscosity (Pa·s)	0.557	0.557	0.557	0.557	0.557
W^{a} (%)	40.00	38.00	36.20	36.20	36.50
A^{d} (%)	26.50	24.05	24.03	23.87	24.15
V^{daf} (%)	23.10	29.10	27.53	30.74	30.45
C^{daf} (%)	87.20	83.51	88.27	85.15	83.11
H^{daf} (%)	5.10	5.19	4.71	5.38	5.22
N^{daf} (%)	2.10	1.91	1.92	1.89	1.92
S^{daf} (%)	1.10	1.00	1.05	0.99	1.01
O^{daf} (%)	4.50	8.39	4.05	6.59	8.74

Table 7. Grid convergence analysis.

Parameters	Grid 1	Grid 2 (Examined)	Grid 3
Number of cells	5625	14,400	360,000
Element size	$4{\cdot}10^{-4}$	$2.5{\cdot}10^{-4}$	$0.5{\cdot}10^{-4}$
Ignition-delay time of composite fuel No. 5 (at 1173 K, V_g = 0), s	1.995	1.990	1.931
GCI (%)	0.062	0.036	0.001

For the computational model, the grid was built in such a way that the value of the maximum size of the grid element was 0.25 mm (14,400 elements in total, 14,641 nodes). In this area of the problem's solution (Figure 4), the ongoing physical and chemical processes were controlled.

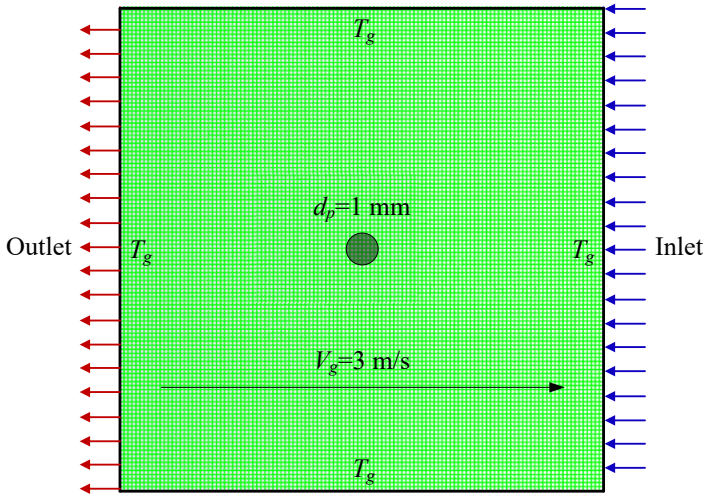

Figure 4. Scheme of the solution domain for ignition in the CLF droplet/air system.

A single droplet injection system was used to generate a CLF droplet with the initial temperature $T_{p,0}$ = 300 K and size d_p = 1 mm. It was placed in the geometric median of the solution domain in Figure 4 (X-position = 0.015 m; Y-position = 0.015 m). At the initial point of time, a uniform distribution of the oxidizer temperature T_g was set. The boundaries of

the solution domain (furnace chamber walls) were described by the first type (Dirichlet) of boundary conditions. The temperatures at the solution domain boundaries were set as constant and equal to T_g according to the experimental data. In the modeling of the composite fuel droplet ignition under the convective heating conditions, the velocity of heated air V_g was 3 m/s. The oxidizer (O_2) concentration was assumed to be equal to the mass content of oxidizer in the air $\varphi_{O_2} = 0.21$.

Verification of the developed mathematical model and assessment of the reliability of the results of numerical simulation were carried out by a standard method for checking the conservatism of the difference scheme used. The step along the temporal and spatial coordinates was chosen by the method of half division until the constancy of the controlled characteristics was achieved. The error of fulfillment of the law of conservation of energy in the area of solution of the ignition problem was calculated at each time step. In the system under consideration, when calculating the ignition characteristics with a step in the spatial coordinate Δr = 250 μm and in time Δt = 25 μs a relatively small error in the performance of the energy balance is achieved (the integral value did not exceed 2.5%).

The target characteristic of the simulated process was the ignition-delay time, which was determined as follows. For t_d we took [73] the period of time from the moment the heating of the fuel droplet began (the beginning of the calculation) until the moment it reached the ignition temperature T_d = 723 K. Figure 5 shows a typical graphical illustration of the determination of the ignition-delay time of the fuel droplet with an initial diameter d_p = 1 mm.

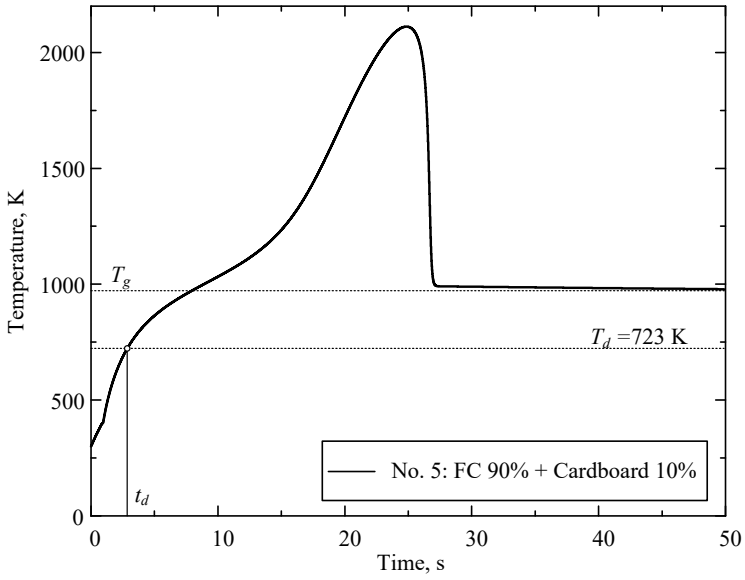

Figure 5. Establishing ignition-delay times by the CLF droplet temperature evolution as illustrated by composition No. 5 (FC 90% + cardboard 10%) at T_g = 973 K, V_g = 0.

3. Results and Discussion

In the numerical simulation, some constants from the source data were not known precisely, thus their values were assumed, on the basis of empirical data, to match the numerical simulation results with the experiment. To establish the main process characteristic (ignition-delay time) as a function of a group of source data, the rates of volatile release from the solid part of the fuel mixture, reaction heat fractions absorbed by the solid and the volatile component fraction/combustible fraction ratios were varied in allowable ranges in Ansys Fluent. Moreover, temperature trends at different heating source temperatures were obtained. The results are presented in Figures 6–9.

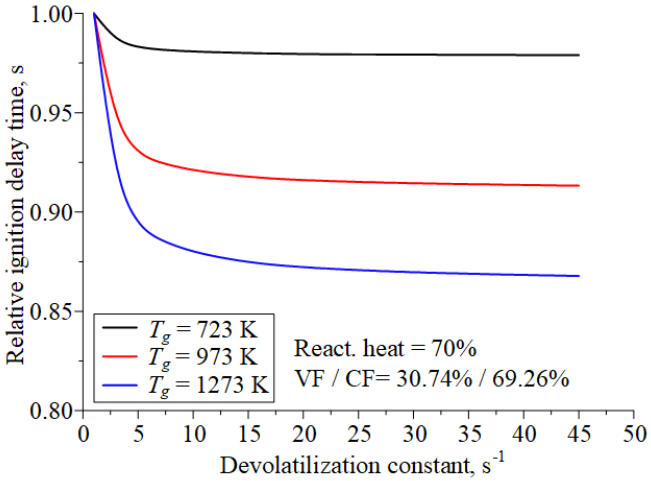

Figure 6. Relative ignition-delay times of CLF No. 4 (FC 90% + plastic 10%) vs. devolatilization constant of the combusting particle at different temperatures of the radiant heating source.

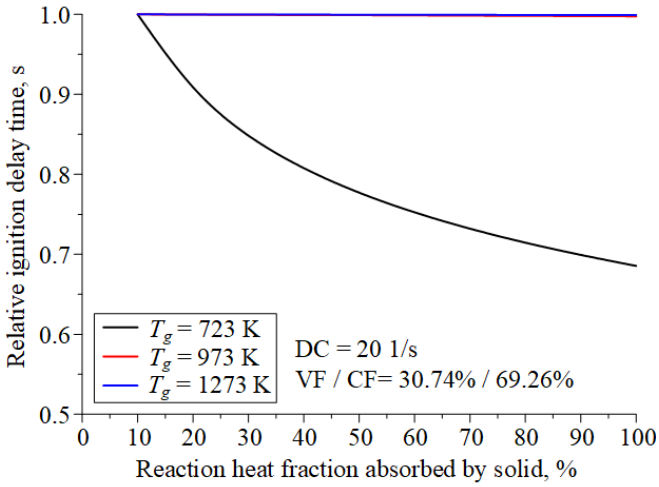

Figure 7. Relative ignition-delay times of CLF No. 4 (FC 90% + plastic 10%) vs. reaction heat fraction absorbed by the solid of the combusting particle at different temperatures of the radiant heating source.

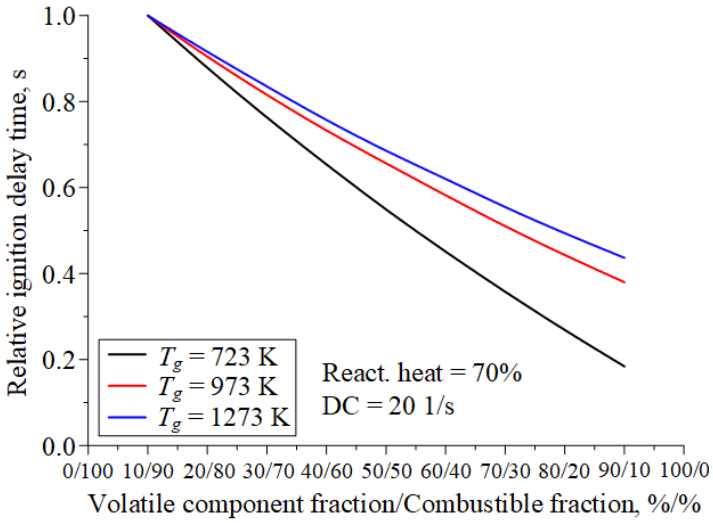

Figure 8. Relative ignition-delay times of CLF vs. volatile component fraction/combustible fraction ratio of the combusting particle at different temperatures of the radiant heating source.

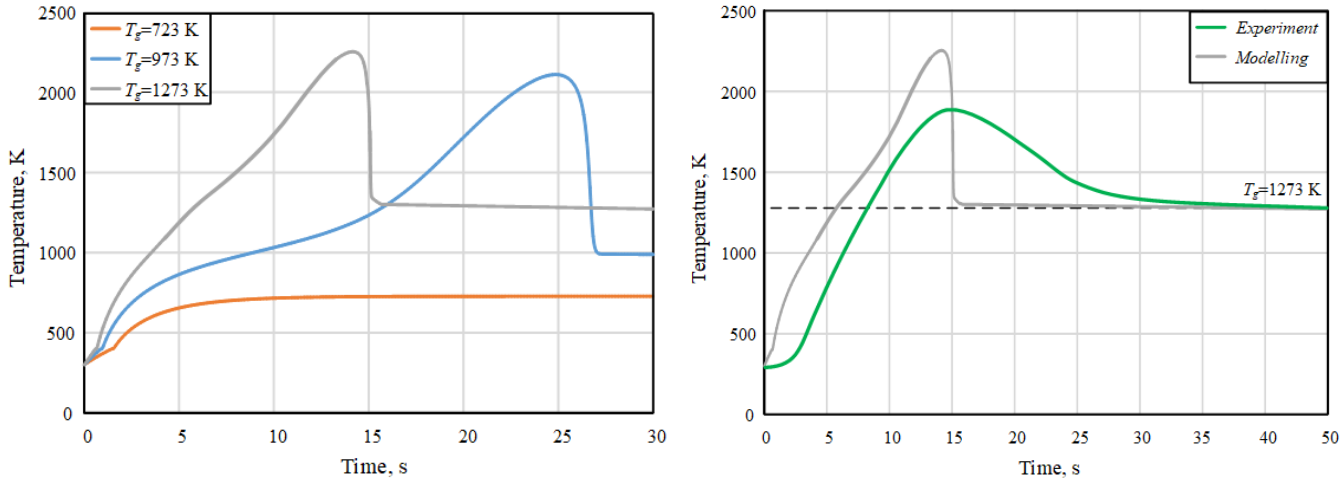

Figure 9. Time dependences of maximum temperature of CLF droplets No. 5 (FC 90% + cardboard 10%) under radiant heating ($V_g \approx 0$): (**a**) simulation results at different heating temperatures; (**b**) simulation results vs. experimental data [41] at T_g = 1273 K.

As seen in Figure 6, changing the devolatilization constant of the combusting particle has a significant impact on the ignition-delay time only when it is varied between 0 and 5 s^{-1}. The ignition-delay time in this condition is an interval from the calculation initiation until the moment the droplet reaches the ignition temperature. Thus, it includes the gas-phase ignition time and the time the solid residue is heated until the ignition temperature (heterogeneous ignition):

$$t_d = t_{gf}(DC) + t_{hg}(T_g) \quad (29)$$

where t_{gf}—gas-phase ignition-delay time of the CLF (depending on the devolatilization rate), s; and t_{hg}—heterogeneous ignition-delay time of the CLF (depending on the ambient air temperature), s.

Thus, the rate of devolatilization affects primarily the fuel gas-phase ignition time (at a constant devolatilization rate, the gas-phase ignition time is constant). Due to the low content of volatiles in the fuel, the time of the gas-phase ignition of the fuel is much shorter compared to the time of heterogeneous ignition. Despite this fact, the influence of this parameter becomes more considerable with an increase in the surrounding oxidizer temperature. The reason for that is that a higher temperature reduces the heterogeneous ignition-delay time, thus increasing the significance of the gas-phase ignition delay which is constant at a constant devolatilization rate.

As the CLF droplet interacts with the heated air, exothermic and endothermic chemical reactions evolve on the surface. Some of the heat they release is absorbed by the fuel solid residue. The higher this value, the faster the solid residue is heated and the lower the ignition-delay time. With the growing ambient temperature, the effect of the absorbed energy from the chemical interaction on the ignition considerably weakens, since the bulk of the energy will come from the radiant and convective heat exchange with the ambient air (Figure 7).

The curves of the CLF ignition-delay times vs. the volatile component fraction/combustible fraction ratio of the combusting particle (Figure 8) are close to linear. The total ignition-delay time diminishes as the combustible fraction decreases. This is because the lower the combustible fraction in the fuel composition, the lower the heterogeneous ignition time which makes up most of the total ignition time of CLF. Moreover, the effect of this ratio is significantly reduced by an increase in the surrounding oxidizer temperature. This pattern is generally confirmed by the experimental research [23]: the higher the temperature, the less influence the heat exchange in the vicinity of the fuel droplet has on the ignition-delay time.

Thus, for better reliability in the prediction of the CLF ignition characteristics with numerical simulation, the data for the volatile component fraction/combustible fraction ratio of the combusting particle need to be determined precisely as source values, whereas the devolatilization constant and reaction heat fractions absorbed by the solid of the combusting particle do not require high accuracy and can be taken from reference materials.

Using the developed mathematical model, the temperature trends of the CLF droplet were obtained during heating, ignition and combustion (Figure 9a) at different temperatures of the heating source (723 K, 973 K and 1273 K). It has been established that the moment at which the maximum temperature is reached shifts to the left with an increase in the temperature of the heating source, which is mainly due to the faster occurrence of a set of physicochemical reactions. The dynamics of the change in the temperature of CLF droplets is of great practical importance, in particular, for the analysis of the energy characteristics of the fuel combustion process. [10,11]. In Figure 9b theoretical and experimental temperature trends are compared. It should be noted that there is a satisfactory qualitative agreement between theory and experiment. At the same time, the quantitative differences are significant and reach more than 20–25%, which is mainly due to the assumptions made in the basic mathematical model. Firstly, constant values of evaporation and devolatilization rates were used in the numerical study. Obviously, under real conditions, the rates of evaporation and devolatilization are not constant, but depend on temperature and change during heating. Second, the model did not take into account the non-uniformity of the temperature distribution inside the CLF droplet and its vicinity, which is the root cause of the change in the rates of physicochemical transformations. Thirdly, the developed model makes it possible to obtain the temperature values directly inside the droplet. The experimental data curve illustrates the temperature in the vicinity of the CLF drop, where the gas mixture burns out, which is formed during the evaporation of the liquid combustible component of the fuel (if present) and during the thermal decomposition of solid components (FC and MSW) [41].

Figure 10 presents the curves of the ignition-delay times vs. oxidizer temperature for CLF with different component compositions. The curves of the ignition-delay times vs. oxidizer temperature are nonlinear. This is conditioned by the fact that, with an increase in temperature, the rates of the thermolysis of organic fuel components, water vaporization, combustion of ignitable gases, and heterogeneous firing of solid remainder change exponentially. This dependence of the ignition-delay times on the ambient temperature was also recorded in the experimental research [23].

Droplets of fuel composition No. 1 (FC 100%) are characterized by maximum ignition-delay times which are due to the high humidity of the initial fuel composition. Induction period of composition No. 1 (Figure 10a) has a longer duration compared with other fuels due to the removal of more energy for the water evaporation. Divergence between the experimental data and the results of numerical simulation for composition No. 1 is 2–43% under radiant heating conditions ($V_g \approx 0$) and 5–32% under convective heating conditions ($V_g \approx 3$ m/s). Differences in ignition-delay times for composition No. 2 (Figure 10b) (FC 90% + wood 10%) over the entire range of temperature variation are 2–48% and 5–29% (with radiant and convective heating, respectively); for other compositions, similar characteristics are as follows: No. 3 (Figure 10c) (FC 90% + rubber 10%)—9–44% and 7–32%; No. 4 (Figure 10d) (FC 90% + plastic 10%)—1–48% and 1–27%; No. 5 (Figure 10e) (FC 90% + cardboard 10%)—10–54% and 3–23%. The last two compositions with the addition of plastic and cardboard (No. 4 and No. 5) are characterized by the most intense ignition of the droplet, which correlates with the experimental data. This is due to the higher content of volatile matter in the fuel composition and its relatively low moisture content. The performed analysis allows us to conclude that the numerical simulation results are in satisfactory agreement with the experimental data.

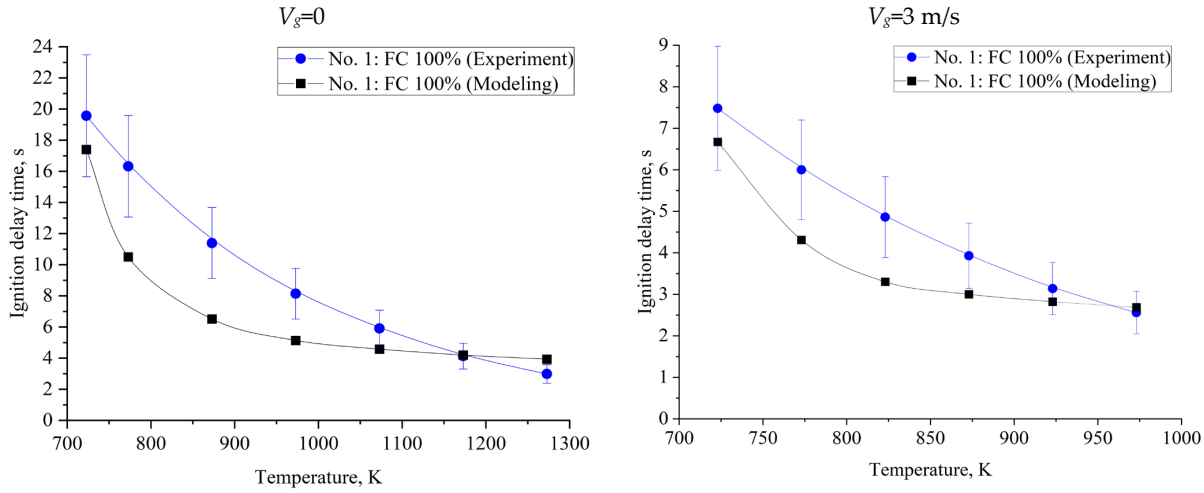

(**a**)

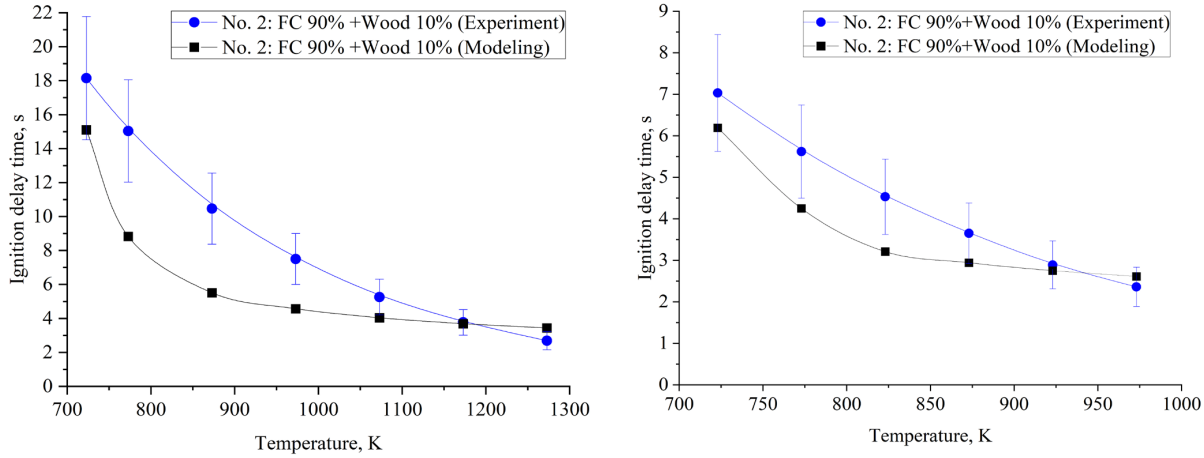

(**b**)

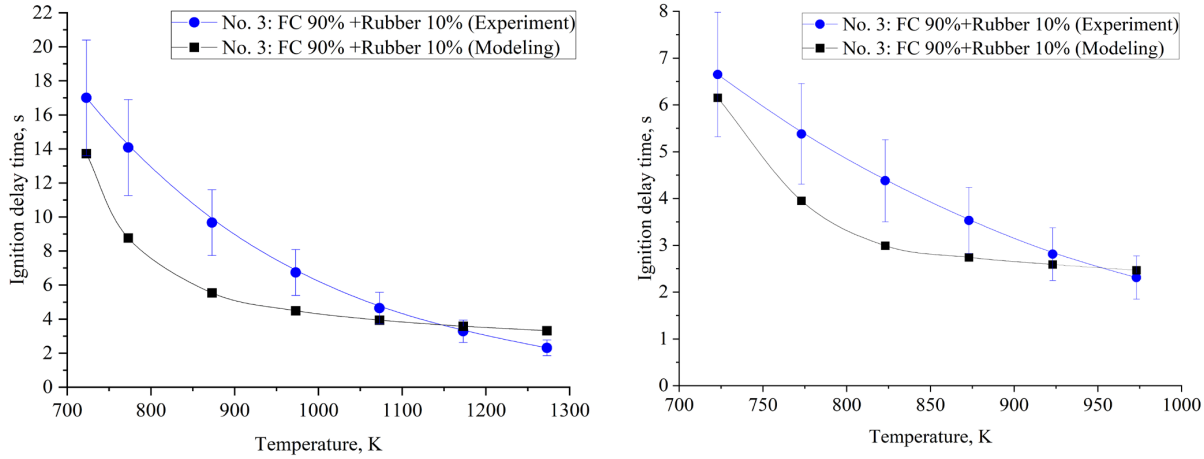

(**c**)

Figure 10. *Cont.*

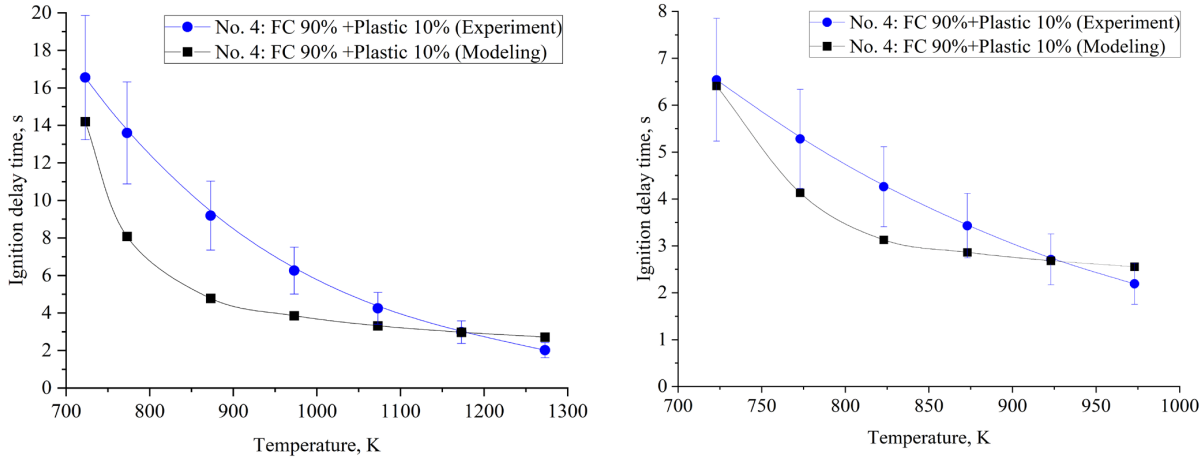

(**d**)

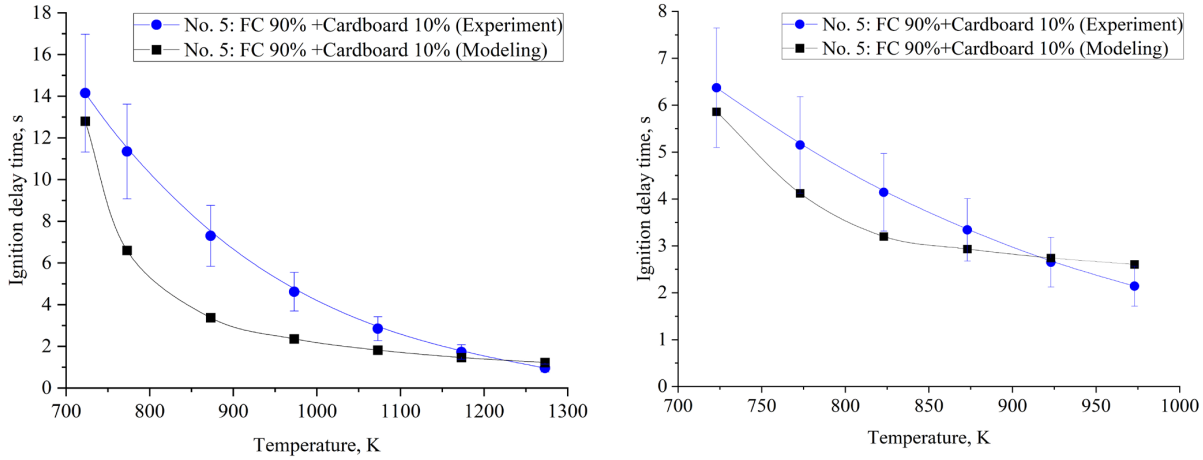

(**e**)

Figure 10. Ignition-delay times vs. heating source temperature at V_g = 0 (left side) and V_g = 3 m/s (right side) for CLF particles of different compositions: (**a**) No. 1 (FC 100%); (**b**) No. 2 (FC 90% + wood 10%); (**c**) No. 3 (FC 90% + rubber 10%); (**d**) No. 4 (FC 90% + plastic 10%); (**e**) No. 5 (FC 90% + cardboard 10%).

It should be noted that the numerical simulation of the processes under study was carried out for somewhat idealized fuel compositions without impurities, which, obviously, is not carried out in practice. We believe that the main differences in the results are due both to the heat losses not taken into account in the model, which are typical during the experiment, and to the occurrence of additional chemical reactions with impurities contained in the real fuel. Impurities can be caused by the content of flotation reagents in coal processing waste (oil refinery products and petrochemical waste). In addition, the combustible MSWs (rubber, wood, plastic) used are chemically complex organic substances, during the combustion of which intermediate components can interact with other fuel components.

The developed mathematical model is most sensitive to a change in the volatile/combustible fraction ratio of the combusting particle. Therefore, for better congruence between the numerical simulation results and experimental data, it is a relevant task to build up an experimental database with reliable experimental values of such constants for different CLF compositions.

An important result of the conducted research is the development of a model that has no limitations on the component composition of fuel slurries and heating conditions. Thus, the model can be applied when the existing power generating facilities are switched to composite fuel. This enables one to evaluate the ignition and combustion characteristics of the fuel, whose properties may vary greatly at different industrial enterprises or within one

enterprise when MSW with a different content of combustible components is used. The model can be used to predict the main integral ignition characteristics of CLF droplets in the operation of current and prospective steam and hot-water boilers. These include, in particular, the ignition-delay times, CLF droplet temperature, fuel component composition changes during heating, unsteady release of volatiles, etc. In the future, the reliability of the numerical simulation results will be improved by integrating user-defined functions (UDF) in the algorithm developed in Ansys Fluent to describe a group of constants, e.g., thermophysical characteristics, as functions of temperature or other external and internal factors.

It should be noted that an increase in the reliability of the results of numerical simulation (Figure 10) can be achieved by taking into account the effect of temperature gradient inside the droplet and in its vicinity. The inhomogeneity of the temperature fields leads to an increase in the duration of the fuel droplet heating period until the moment of ignition in comparison with the previously described idealized ignition problem. However, the description of transient heat transfer processes requires large computing power of the PC.

4. Effect of Temperature Gradient Inside the Droplet and in Its Vicinity

This section presents the first results on the modernization of the developed mathematical model for a more reliable description of the experimental data. Compared to the base model (1)–(28), the advanced version of the model additionally takes into account the non-uniform temperature distribution inside the CLF droplet according to the heat transfer equation:

$$\frac{\partial T_p}{\partial t} = a_p \left(\frac{\partial^2 T_p}{\partial r^2} + \frac{2}{r} \frac{\partial T_p}{\partial r} \right) \quad (30)$$

where r—droplet radius in spherical coordinates, m; T_p—droplet temperature, K; and a_p—thermal diffusivity of CLF, m^2/s.

The complexity of the mathematical model made it possible to construct typical temperature fields for solving the problem of ignition of a CLF droplet for qualitative comparison with videograms of experimental studies [23] (Figure 11). The first case (Figure 11a) was radiant heating ($V_g \approx 0$). The second case (Figure 11b) was convective heating ($V_g \approx 3$ m/s). As can be seen, there is a qualitative agreement between experimental data and simulation results in the stages of industrial waste-derived fuel droplet combustion: passive warming, near-surface water vaporization, thermolysis of coal and municipal waste (solid combustible components), blending of ignitable gases with the oxidizing medium, gas blend firing and burnout, and heating of the solid remainder followed by its heterogeneous ignition and combustion.

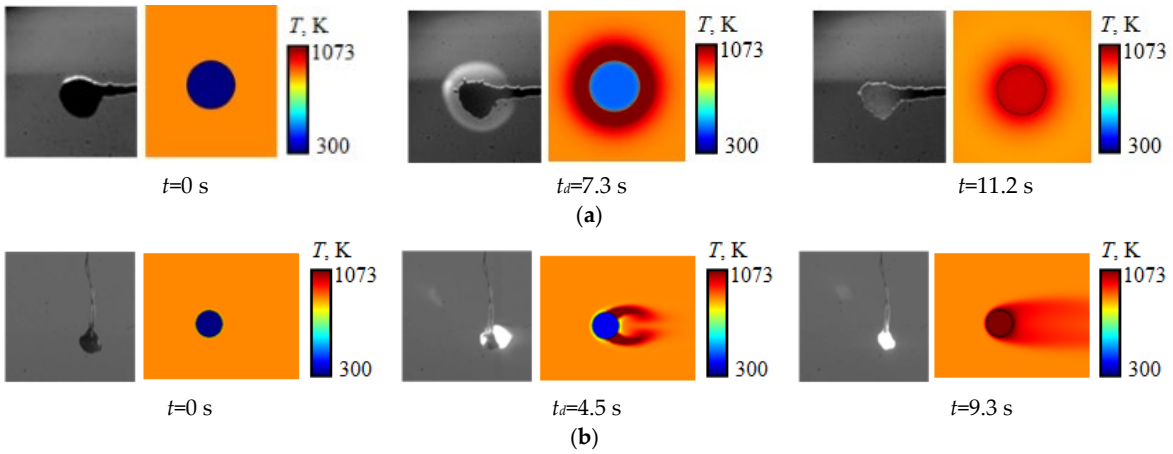

Figure 11. Temperature fields and videoframes obtained in experiments of ignition and combustion of CLF droplets No. 5 (FC 90% + cardboard 10%) at T_g = 873 K [23] under the following conditions: (**a**) radiant heating ($V_g \approx 0$); (**b**) convective heating ($V_g \approx 3$ m/s).

Using the advanced mathematical model, ignition-delay times t_d are determined depending on the temperature of the heating source T_g. Satisfactory agreement between experiment and theory was obtained (Figure 12). In this case, the difference in the results for t_d over the entire range of temperatures under study does not exceed 19% both under conditions of radiant heating (Figure 12a) and convective heating (Figure 12b), which does not exceed the confidence limit for the obtained experimental data [23].

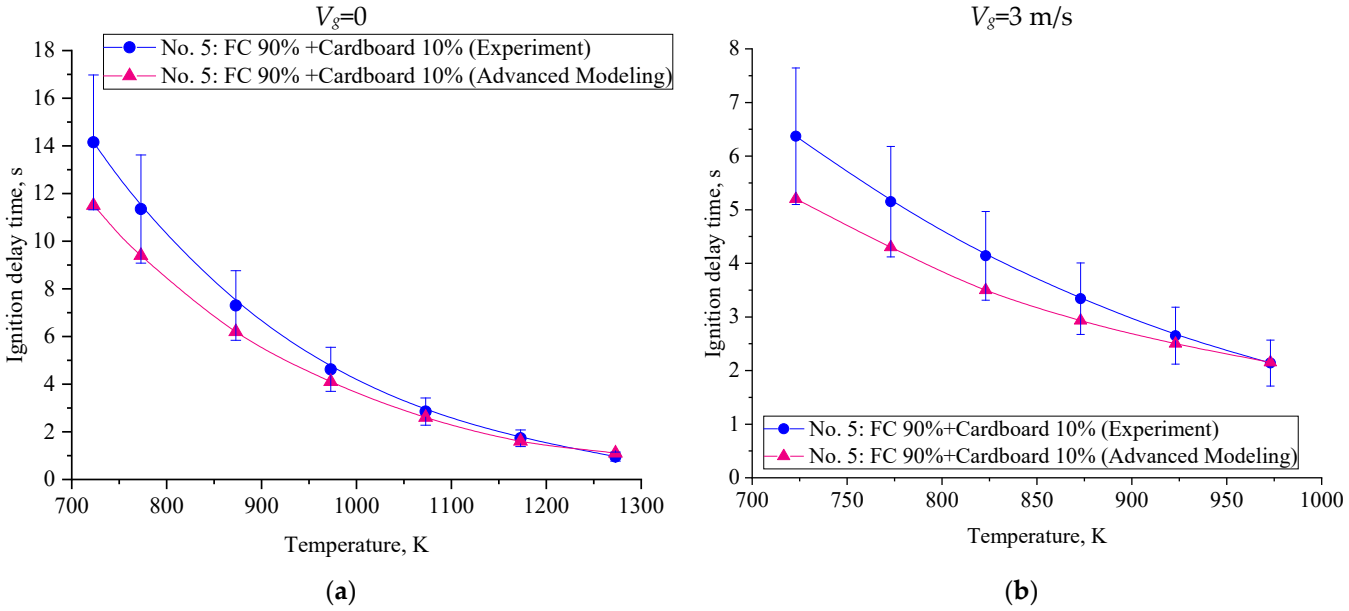

Figure 12. Ignition-delay times vs. heating source temperature for CLF composition No. 5 (FC 90% + cardboard 10%) at: (**a**) V_g = 0; (**b**) V_g = 3 m/s.

It should be noted that when the non-uniform temperature distribution inside a single CLF droplet and in its vicinity is taken into account, the PC calculation times increase by a factor of 5–10. On the scale of the steam boiler, there will be an exponential increase in the PC calculation times. On the scale of the steam boiler, there will be an exponential increase in the PC calculation times. The relatively simple modernization performed on the mathematical model, on the one hand, leads to a satisfactory agreement between the results of numerical simulation and experimental data, but, on the other hand, requires large computing power. The most rational approach in practical applications is the development of a mathematical model with maximum simplifications but with acceptable reproducibility of experimental data.

5. Conclusions

Based on results of previous experimental studies, a mathematical model was developed for the ignition and combustion of a single composite liquid fuel droplet (a mixture of coal processing waste in a wet state with combustible municipal solid waste). The model considers the interdependent sequence of the main chemical transformations and physical interactions of the suspended CLF droplet with the surrounding air environment (passive warming, near-surface water vaporization, thermolysis of coal and municipal waste (solid combustible components), blending of ignitable gases with the oxidizing medium, gas blend firing and burnout, and heating of the solid remainder followed by its heterogeneous ignition and combustion with an ash residue formation) as a result of combined radiant and convective heat transfer, the heating source temperature for which was varied within the ranges of 723–1273 K and 723–973 K, respectively. The numerical simulation of combustion characteristics was carried out in the Ansys Fluent commercial software for five different CLF compositions. Comparison of the ignition-delay times for single droplets obtained by numerical simulation with experimental data showed their good

agreement for mathematical model configuration, considering the temperature gradient inside the fuel droplet and in its vicinity. The results of numerical simulation of a CLF droplet in a heated air flow differ from the experimental data by no more than 19%, both under conditions of radiant heating and convective heating, which does not exceed the confidence limit for the obtained experimental data. The developed mathematical model of the ignition and combustion process of a single CLF droplet makes it possible to predict the main characteristics with good reliability. The mathematical model is most sensitive to changes in the ratio of volatile/combustible fractions of the combusting particle, therefore, an urgent task in the improvement of the correspondence of numerical simulation results with experimental data is to compile an information base with reliable experimental values of such constants for different CLF compositions. It can also be noted that the predictive mechanism developed in Ansys Fluent can significantly reduce the time and material costs of subsequent research.

Author Contributions: Conceptualization, D.G.; data curation, A.R.; formal analysis, D.A.; funding acquisition, D.G.; investigation, K.P.; methodology, D.A.; project administration, K.P.; writing—original draft, K.P.; writing—review and editing, D.K. All authors have read and agreed to the published version of the manuscript.

Funding: This work was supported by the Russian Foundation for Basic Research, National Council of Brazil for Scientific and Technological Development and Ministry of Science & Technology (Government of India) grant number [19-53-80019].

Institutional Review Board Statement: Not applicable.

Informed Consent Statement: Not applicable.

Conflicts of Interest: The authors declare no conflict of interest. The funders had no role in the design of the study; in the collection, analyses, or interpretation of data; in the writing of the manuscript; or in the decision to publish the results.

Abbreviations

CF	combustible fraction
CLF	composite liquid fuel
DC	devolatilization constant
DPM	discrete particle model
FC	filter cake
MSW	municipal solid waste
RANS	Reynolds-averaged Navier-Stokes equations
TPP	thermal power plant
VF	volatile fraction

Nomenclature

A^{d}	ash content, %
a_p	thermal diffusivity of CLF, m^2/s
A_p	surface area of the droplet, m^2
A_r	pre-exponential factor
A_0	rate constant, s^{-1}
C_D	drag coefficient for spherical droplet
C^{daf}, H^{daf}, N^{daf}, O^{daf}, S^{daf}	fraction of carbon, hydrogen, nitrogen, oxygen, sulfur in the sample converted to a dry ash free state, %
$C_{d,b}$, $C_{d,s}$	concentration of the diffusion-limited species
$C_{i,s}$	vapor concentration at the droplet surface, $kg{\cdot}mol/m^3$
$C_{i,\infty}$	vapor concentration in the bulk gas, $kg{\cdot}mol/m^3$
C_k	concentrations of all other species
c_p	particle (droplet) heat capacity, J/(kg·K)
$c_{p,\infty}$	gas heat capacity, J/(kg·K)

$C_{1,r}$	molar concentration of species j in reactions, mol
$D_{i,m}$	diffusion coefficient of vapor in the bulk, m^2/s
d_p	particle (droplet) diameter, m
$D_{0,r}$	diffusion rate coefficient for reaction
E_r	activation energy for reaction, J/(mol·K)
$\vec{F}$	vector of volumetric fluid / particle interaction force, N
F_a	additional acceleration, N/kg
F_D	coefficient in drag law, 1/s
f_h	particle fraction which absorbs heat of reaction
$f_{v,0}$	initial mass fraction of volatiles
$f_{w,0}$	initial mass fraction of evaporating material
$\vec{g}$	gravity acceleration, m/s^2
G_k	generation of turbulence kinetic energy related to the mean velocity gradient and the turbulent model constants
H	enthalpy, W
h	convective heat transfer coefficient, $W/(m^2 \cdot K)$
h_{fg}	latent heat, J/kg
h_i	sensible heat, W
H_{reac}	heat released by the surface reaction, J/kg
$\vec{J}$	mass flux, $kg/(m^2 \cdot s)$
k	turbulent kinetic energy, m^2/s^2
k_c	mass transfer coefficient, m/s
k_∞	thermal conductivity of the gas, W/(m·K)
m_p	particle (droplet) mass, kg
$m_{p,0}$	initial particle (droplet) mass, kg
$M_{w,i}$	molecular weight of species i, kg/mol·K
N_i	molar flux of vapor, $kg \cdot mol/(m^2 \cdot s)$
N_r	apparent order of reaction
Nu	Nusselt number
p	gas local absolute pressure, Pa
p_n	bulk partial pressure of the gas phase species, Pa
Pr	Prandtl number
$p_{r,d}$	bulk partial pressure of the diffusion-limited species, Pa
p_{sat}	saturated vapor pressure, Pa
Q	heat of combustion, J/kg
$Q^a{}_{s,V}$	higher heating value, J/kg
r	droplet radius in spherical coordinates, m
R	the universal gas constant, J/(K·mol)
R_p	rate of production, units vary
Re	relative Reynolds number
$\overline{R}_{j,r}$	rate of particle surface species depletion, kg/s
$R_{j,r}$	rate of particle surface species reaction per unit area, $kg/(m^2 \cdot s)$
$R_{kin,r}$	kinetic rate of reaction, units vary
Sc	Schmidt number
Sh	Sherwood number
t	time, s
T_{bp}	boiling point, K
T_d	CLF ignition temperature, K
t_d	ignition delay time, s
T_g	oxidizer temperature, K
t_{gf}	gas-phase ignition-delay time, s
t_{hg}	heterogeneous ignition-delay time of CLF, s
T_p	droplet temperature, K
$T_{p,0}$	initial particle (droplet) temperature, K
T_{vap}	vaporization temperature, K
T_∞	gas temperature, K
$\vec{u}$	velocity vector, m/s
u	gas velocity, m/s

u_p	particle velocity, m/s
V^{daf}	volatile content, %
V_g	oxidizer velocity, m/s
W^a	moisture content, %
X_i	local bulk mole fraction of species i
Y	mass fraction of solid fuel
Y_j	mass fraction of surface species j in the particle
Greek symbols	
β_r	temperature exponent
Δr	step on spatial coordinate, m
Δt	time step, s
ε	turbulent dissipation rate, m^2/s^3
ε_p	particle emissivity
η_r	effectiveness factor
θ_R	radiation temperature, K
μ	gas dynamic viscosity, Pa·s
μ_t	turbulent dynamic viscosity, Pa·s
ρ	gas density, kg/m^3
ρ_p	particle (droplet) density, kg/m^3
σ	Stefan-Boltzmann constant, $W/(m^2 \cdot K^4)$
σ_k	turbulent Prandtl number for turbulent kinetic energy
σ_ε	turbulent Prandtl number for turbulent dissipation rate
$\overline{\tau}$	gas viscous stress, Pa
φ_{O_2}	mass content of oxygen in the air
Subscripts	
i	species
n	number of gas phase specie

References

1. Khan, H.H.; Malik, M.N.; Zafar, R.; Goni, F.A.; Chofreh, A.G.; Klemeš, J.J.; Alotaibi, Y. Challenges for Sustainable Smart City Development: A Conceptual Framework. *Sustain. Dev.* **2020**, *28*, 1507–1518. [CrossRef]
2. IEA World Energy Outlook 2020. Available online: https://iea.blob.core.windows.net/assets/a72d8abf-de08-4385-8711-b8a062d6124a/WEO2020.pdf (accessed on 1 March 2021).
3. Global Information Inc. *Global Industrial Waste Management Market-2019–2026*; Global Information Inc.: Tokyo, Japan, 2020.
4. Gupta, A.; Paranjape, N. *Industrial Solid Waste Management Market 2020–2026*; Global Market Insights Inc.: Selbyville, DE, USA, 2020.
5. Kaza, S.; Yao, L.C.; Bhada-Tata, P.; Van Woerden, F. *What a Waste 2.0: A Global Snapshot of Solid Waste Management to 2050*; World Bank: Washington, DC, USA, 2018; ISBN 978-1-4648-1329-0.
6. Sabour, M.R.; Alam, E.; Hatami, A.M. Global Trends and Status in Landfilling Research: A Systematic Analysis. *J. Mater. Cycles Waste Manag.* **2020**, *22*, 711–723. [CrossRef]
7. Chen, D.M.C.; Bodirsky, B.L.; Krueger, T.; Mishra, A.; Popp, A. The World's Growing Municipal Solid Waste: Trends and Impacts. *Environ. Res. Lett.* **2020**, *15*, 074021. [CrossRef]
8. Xin, C.; Zhang, T.; Tsai, S.-B.; Zhai, Y.-M.; Wang, J. An Empirical Study on Greenhouse Gas Emission Calculations under Different Municipal Solid Waste Management Strategies. *Appl. Sci.* **2020**, *10*, 1673. [CrossRef]
9. Han, Z.; Wang, S.; Zhao, J.; Hu, X.; Fei, Y.; Xu, M. Identification of Nitrogen-Sources in an Aquifer beneath a Municipal Solid Waste Landfill in the Vicinity of Multiple Pollutant Sources. *J. Environ. Manag.* **2020**, *268*, 110661. [CrossRef] [PubMed]
10. Foster, W.; Azimov, U.; Gauthier-Maradei, P.; Molano, L.C.; Combrinck, M.; Munoz, J.; Esteves, J.J.; Patino, L. Waste-to-Energy Conversion Technologies in the UK: Processes and Barriers–A Review. *Renew. Sustain. Energy Rev.* **2021**, *135*, 110226. [CrossRef]
11. Glushkov, D.O.; Strizhak, P.A. Ignition of Composite Liquid Fuel Droplets Based on Coal and Oil Processing Waste by Heated Air Flow. *J. Clean. Prod.* **2017**, *165*, 1445–1461. [CrossRef]
12. Staroń, A.; Kowalski, Z.; Staroń, P.; Banach, M. Studies on CWL with Glycerol for Combustion Process. *Environ. Sci. Pollut. Res.* **2019**, *26*, 2835–2844. [CrossRef] [PubMed]
13. Zhao, Z.; Wang, R.; Ge, L.; Wu, J.; Yin, Q.; Wang, C. Energy Utilization of Coal-Coking Wastes via Coal Slurry Preparation: The Characteristics of Slurrying, Combustion, and Pollutant Emission. *Energy* **2019**, *168*, 609–618. [CrossRef]
14. Aliukov, S.; Osintsev, K. Mathematical Modeling of Coal Dust Screening by Means of Sieve Analysis and Coal Dust Combustion Based on New Methods of Piece-linear Function Approximation. *Appl. Sci.* **2021**, *11*, 1609. [CrossRef]
15. Sun, W.; Zhong, W.; Zhang, J.; Echekki, T. Large Eddy Simulation on the Effects of Coal Particles Size on Turbulent Combustion Characteristics and NOx Formation inside a Corner-Fired Furnace. *J. Energy Resour. Technol.* **2021**, *143*, 082302. [CrossRef]
16. Gu, T.; Yin, C.; Ma, W.; Chen, G. Municipal Solid Waste Incineration in a Packed Bed: A Comprehensive Modeling Study with Experimental Validation. *Appl. Energy* **2019**, *247*, 127–139. [CrossRef]

17. Janajreh, I.; Adeyemi, I.; Elagroudy, S. Gasification Feasibility of Polyethylene, Polypropylene, Polystyrene Waste and Their Mixture: Experimental Studies and Modeling. *Sustain. Energy Technol. Assess.* **2020**, *39*, 100684. [CrossRef]
18. Bahari, A.; Atashkari, K.; Mahmoudimehr, J. Multi-Objective Optimization of a Municipal Solid Waste Gasifier. *Biomass Convers. Biorefinery* **2020**, *11*, 1703–1718. [CrossRef]
19. Somwangthanaroj, S.; Fukuda, S. Investigation of Multi-Fuel Combustion Behavior and Synergy Effect Using Improved Steady-State Discrete Particle Model Simulation. *Int. J. Energy Res.* **2020**, *45*, 17291–17301. [CrossRef]
20. Zhuo, Y.; Shen, Y. Three-Dimensional Transient Modelling of Coal and Coke Co-Combustion in the Dynamic Raceway of Ironmaking Blast Furnaces. *Appl. Energy* **2020**, *261*, 114456. [CrossRef]
21. Tokmurzin, D.; Adair, D. Development of Euler-Lagrangian Simulation of a Circulating Fluidized Bed Reactor for Coal Gasification. *Eurasian Chem. J.* **2019**, *21*, 45–49. [CrossRef]
22. Yang, R.; Ma, C.; Chen, G.; Cheng, Z.; Yan, B.; Mansour, M. Study on NOx Emission during Corn Straw/Sewage Sludge Co-Combustion: Experiments and Modelling. *Fuel* **2021**, *285*, 119208. [CrossRef]
23. Glushkov, D.O.; Paushkina, K.K.; Shabardin, D.P.; Strizhak, P.A. Environmental Aspects of Converting Municipal Solid Waste into Energy as Part of Composite Fuels. *J. Clean. Prod.* **2018**, *201*, 1029–1042. [CrossRef]
24. Glushkov, D.O.; Feoktistov, D.V.; Kuznetsov, G.V.; Batishcheva, K.A.; Kudelova, T.; Paushkina, K.K. Conditions and Characteristics of Droplets Breakup for Industrial Waste-Derived Fuel Suspensions Ignited in High-Temperature Air. *Fuel* **2020**, *265*, 116915. [CrossRef]
25. Nyashina, G.S.; Legros, J.C.; Strizhak, P.A. Environmental Potential of Using Coal-Processing Waste as the Primary and Secondary Fuel for Energy Providers. *Energies* **2017**, *10*, 405. [CrossRef]
26. Nyashina, G.S.; Kuznetsov, G.V.; Strizhak, P.A. Energy Efficiency and Environmental Aspects of the Combustion of Coal-Water Slurries with and without Petrochemicals. *J. Clean. Prod.* **2018**, *172*, 1730–1738. [CrossRef]
27. Nyashina, G.S.; Kurgankina, M.A.; Strizhak, P.A. Environmental, Economic and Energetic Benefits of Using Coal and Oil Processing Waste Instead of Coal to Produce the Same Amount of Energy. *Energy Convers. Manag.* **2018**, *174*, 175–187. [CrossRef]
28. Glushkov, D.O.; Paushkina, K.K.; Shabardin, D.P.; Strizhak, P.A.; Gutareva, N.Y. Municipal Solid Waste Recycling by Burning It as Part of Composite Fuel with Energy Generation. *J. Environ. Manag.* **2019**, *231*, 896–904. [CrossRef] [PubMed]
29. Moriguchi, Y.; Hashimoto, S. Material Flow Analysis and Waste Management. In *Taking Stock of Industrial Ecology*; Springer International Publishing: Cham, Switzerland, 2016; pp. 247–262. ISBN 9783319205717.
30. Edjabou, M.E.; Martín-Fernández, J.A.; Scheutz, C.; Astrup, T.F. Statistical Analysis of Solid Waste Composition Data: Arithmetic Mean, Standard Deviation and Correlation Coefficients. *Waste Manag.* **2017**, *69*, 13–23. [CrossRef] [PubMed]
31. Faitli, J.; Magyar, T.; Erdélyi, A.; Murányi, A. Characterization of Thermal Properties of Municipal Solid Waste Landfills. *Waste Manag.* **2015**, *36*, 213–221. [CrossRef] [PubMed]
32. Birgen, C.; Magnanelli, E.; Carlsson, P.; Skreiberg, Ø.; Mosby, J.; Becidan, M. Machine Learning Based Modelling for Lower Heating Value Prediction of Municipal Solid Waste. *Fuel* **2021**, *283*, 118906. [CrossRef]
33. Wang, D.; Tang, Y.T.; He, J.; Yang, F.; Robinson, D. Generalized Models to Predict the Lower Heating Value (LHV) of Municipal Solid Waste (MSW). *Energy* **2021**, *216*, 119279. [CrossRef]
34. Tabakaev, R.; Shanenkov, I.; Kazakov, A.; Zavorin, A. Thermal Processing of Biomass into High-Calorific Solid Composite Fuel. *J. Anal. Appl. Pyrolysis* **2017**, *124*, 94–102. [CrossRef]
35. Ilinykh, G.V. Evaluation of Thermotechnical Properties of Solid Waste from Their Morphological Composition. *Vestn. Permsk. Natsionalnogo Issledovatelskogo Politekh. Univ. Urban.* **2013**, *11*, 125–137.
36. Glushkov, D.O.; Strizhak, P.A.; Chernetskii, M.Y. Organic Coal-Water Fuel: Problems and Advances (Review). *Therm. Eng.* **2016**, *63*, 707–717. [CrossRef]
37. Glushkov, D.O.; Shabardin, D.P.; Strizhak, P.A.; Vershinina, K.Y. Influence of Organic Coal-Water Fuel Composition on the Characteristics of Sustainable Droplet Ignition. *Fuel Process. Technol.* **2016**, *143*, 60–68. [CrossRef]
38. Dmitrienko, M.A.; Strizhak, P.A.; Tsygankova, Y.S. Technoeconomic Analysis of Prospects of Use of Organic Coal-Water Fuels of Various Component Compositions. *Chem. Pet. Eng.* **2017**, *53*, 195–202. [CrossRef]
39. Stöllinger, M.; Naud, B.; Roekaerts, D.; Beishuizen, N.; Heinz, S. PDF Modeling and Simulations of Pulverized Coal Combustion-Part 1: Theory and Modeling. *Combust. Flame* **2013**, *160*, 384–395. [CrossRef]
40. Lyulin, Y.V.; Feoktistov, D.V.; Afanas'ev, I.A.; Chachilo, E.S.; Kabov, O.A.; Kuznetsov, G.V. Measuring the Rate of Local Evaporation from the Liquid Surface under the Action of Gas Flow. *Tech. Phys. Lett.* **2015**, *41*, 665–667. [CrossRef]
41. Glushkov, D.O.; Paushkina, K.K.; Shabardin, D.P. Co-Combustion of Coal Processing Waste, Oil Refining Waste and Municipal Solid Waste: Mechanism, Characteristics, Emissions. *Chemosphere* **2020**, *240*, 124892. [CrossRef]
42. ANSYS Academic Research ANSYS Fluent Theory Guide. In *ANSYS Help System*; ANSYS, Inc.: Canonsburg, PA, USA, 2018.
43. Ranz, W.E.; Marshall, W.R. Evaporation From Drops–Part I. *Chem. Eng. Prog.* **1952**, *48*, 141–146.
44. Aissa, A.; Abdelouahab, M.; Noureddine, A.; Elganaoui, M.; Pateyron, B. Ranz and Marshall Correlations Limits on Heat Flow between a Sphere and Its Surrounding Gas at High Temperature. *Therm. Sci.* **2015**, *19*, 1521–1528. [CrossRef]
45. Baum, M.M.; Street, P.J. Predicting the Combustion Behaviour of Coal Particles. *Combust. Sci. Technol.* **1971**, *3*, 231–243. [CrossRef]
46. Wijayanta, A.T.; Alam, M.S.; Nakaso, K.; Fukai, J.; Kunitomo, K.; Shimizu, M. Combustibility of Biochar Injected into the Raceway of a Blast Furnace. *Fuel Process. Technol.* **2014**, *117*, 53–59. [CrossRef]

47. Ejeh, C.; Afgan, I.; AlMansob, H.; Brantson, E.; Fekala, J.; Odiator, M.; Stanley, P.; Anumah, P.; Onyekperem, C.; Boah, E. Computational Fluid Dynamics for Ameliorating Oil Recovery Using Silicon-Based Nanofluids and Ethanol in Oil-Wet Reservoirs. *Energy Rep.* **2020**, *6*, 3023–3035. [CrossRef]
48. Glushkov, D.O.; Kuznetsov, G.V.; Paushkina, K.K.; Shabardin, D.P. The Main Elements of a Strategy for Combined Utilization of Industrial and Municipal Waste from Neighboring Regions by Burning It as Part of Composite Fuels. *Energies* **2018**, *11*, 2534. [CrossRef]
49. Taghiyeva, S.F.; Jafarov, R.P.; Kasimov, A.A.; Qadji-Kasumov, V.S.; Rustamov, M.I. Kinetic Model of Hydrogenation of Carbon Dioxide on the Catalyst Fe, Ni/γ-Al2O3. *PPOR* **2017**, *18*, 62–68.
50. Wickramaarachchi, W.A.M.K.P.; Narayana, M. Pyrolysis of Single Biomass Particle Using Three-Dimensional Computational Fluid Dynamics Modelling. *Renew. Energy* **2020**, *146*, 1153–1165. [CrossRef]
51. Wei, X.; Zhong, H.; Yang, Q.; Yao, E.; Zhang, Y.; Zou, H. Studying the Mechanisms of Natural Rubber Pyrolysis Gas Generation Using RMD Simulations and TG-FTIR Experiments. *Energy Convers. Manag.* **2019**, *189*, 143–152. [CrossRef]
52. Vatani, A.; Mehrpooya, M.; Gharagheizi, F. Prediction of Standard Enthalpy of Formation by a QSPR Model. *Int. J. Mol. Sci.* **2007**, *8*, 407–432. [CrossRef]
53. Parks, G.S.; Mosher, H.P. Enthalpy and Free Energy Changes in Some Simple Polymerization Processes. *J. Polym. Sci. Part A Gen. Pap.* **1963**, *1*, 1979–1984. [CrossRef]
54. Salomatov, V.V.; Kuznetsov, G.V.; Syrodoy, S.V. Influence of the Degree of Coal Metamorphism on Characteristics and Conditions of Ignition of Coal-Water Fuel Drops. *Thermophys. Aeromechanics* **2018**, *25*, 773–788. [CrossRef]
55. Arena, U. Process and Technological Aspects of Municipal Solid Waste Gasification. A Review. *Waste Manag.* **2012**, *32*, 625–639. [CrossRef] [PubMed]
56. Guan, Y.; Luo, S.; Liu, S.; Xiao, B.; Cai, L. Steam Catalytic Gasification of Municipal Solid Waste for Producing Tar-Free Fuel Gas. *Int. J. Hydrogen Energy* **2009**, *34*, 9341–9346. [CrossRef]
57. Donskoy, I.G. Numerical Study on the Efficiency of Biomass and Municipal Waste Fixed-Bed Co-Gasification. *E3S Web Conf.* **2019**, *114*, 06006. [CrossRef]
58. Xie, J.; Zhong, W.; Jin, B.; Shao, Y.; Huang, Y. Eulerian–Lagrangian Method for Three-Dimensional Simulation of Fluidized Bed Coal Gasification. *Adv. Powder Technol.* **2013**, *24*, 382–392. [CrossRef]
59. Chen, C.J.; Hung, C.I.; Chen, W.H. Numerical Investigation on Performance of Coal Gasification under Various Injection Patterns in an Entrained Flow Gasifier. *Appl. Energy* **2012**, *100*, 218–228. [CrossRef]
60. He, C.; Feng, X.; Chu, K.H.; Li, A.; Liu, Y. Industrial-Scale Fixed-Bed Coal Gasification: Modeling, Simulation and Thermodynamic Analysis. *Chin. J. Chem. Eng.* **2014**, *22*, 522–530. [CrossRef]
61. Haseli, Y.; van Oijen, J.A.; de Goey, L.P.H. A Detailed One-Dimensional Model of Combustion of a Woody Biomass Particle. *Bioresour. Technol.* **2011**, *102*, 9772–9782. [CrossRef] [PubMed]
62. Zhang, Q.; Dor, L.; Fenigshtein, D.; Yang, W.; Blasiak, W. Gasification of Municipal Solid Waste in the Plasma Gasification Melting Process. *Appl. Energy* **2012**, *90*, 106–112. [CrossRef]
63. Uskov, S.I.; Enikeeva, L.V.; Potemkin, D.I.; Belyaev, V.D.; Snytnikov, P.V.; Gubaidullin, I.M.; Kirillov, V.A.; Sobyanin, V.A. Kinetics of Low-Temperature Steam Reforming of Propane in a Methane Excess on a Ni-Based Catalyst. *Catal. Ind.* **2017**, *9*, 104–109. [CrossRef]
64. McAllister, S.; Chen, J.-Y.; Fernandez-Pello, A.C. Chemical Kinetics. In *Fundamentals of Combustion Processes*; Springer: New York, NY, USA, 2011; pp. 49–73.
65. Matthess, N.; Schweich, D.; Martin, B.; Castagna, F. From Light-off Curves to Kinetic Rate Expressions for Three-Way Catalysts. *Top. Catal.* **2001**, *16–17*, 119–124. [CrossRef]
66. Westbrook, C.K.; Dryer, F.L. Chemical Kinetic Modeling of Hydrocarbon Combustion. *Prog. Energy Combust. Sci.* **1984**, *10*, 1–57. [CrossRef]
67. Mendoza, J.A.; Hwang, S. Tubular Reactor Design for the Oxidative Dehydrogenation of Butene Using Computational Fluid Dynamics (CFD) Modeling. *Korean J. Chem. Eng.* **2018**, *35*, 2157–2163. [CrossRef]
68. Cheng, G.; Farmer, R.; Jones, H.; McFarlane, J. Numerical Simulation of the Internal Ballistics of a Hybrid Rocket Motor. In Proceedings of the 32nd Aerospace Sciences Meeting and Exhibit, Reno, NV, USA, 10–13 January 1994; American Institute of Aeronautics and Astronautics: Reston, VA, USA, 1994.
69. Tao, F.; Srinivas, S.; Reitz, R.D.; Foster, D.E. Comparison of Three Soot Models Applied to Multi-Dimensional Diesel Combustion Simulations. *JSME Int. J. Ser. B* **2005**, *48*, 671–678. [CrossRef]
70. McAllister, S.; Chen, J.-Y.; Fernandez-Pello, A.C. Droplet Evaporation and Combustion. In *Fundamentals of Combustion Processes*; Springer: New York, NY, USA, 2011; pp. 155–175.
71. Celik, I.B.; Ghia, U.; Roache, P.J.; Freitas, C.J.; Coleman, H.; Raad, P.E. Procedure for Estimation and Reporting of Uncertainty Due to Discretization in CFD Applications. *J. Fluids Eng. Trans. ASME* **2008**, *130*, 0780011–0780014. [CrossRef]
72. Fugmann, H.; Schnabel, L.; Frohnapfel, B. Heat Transfer and Pressure Drop Correlations for Laminar Flow in an In-Line and Staggered Array of Circular Cylinders. *Numer. Heat Transf. Part A Appl.* **2019**, *75*, 1–20. [CrossRef]
73. Glushkov, D.O.; Strizhak, P.A.; Vershinina, K.Y. Minimum Temperatures for Sustainable Ignition of Coal Water Slurry Containing Petrochemicals. *Appl. Therm. Eng.* **2016**, *96*, 534–546. [CrossRef]